Energy LAB

RESEARCH ARTICLE

Energy Lab 2023, 1, 220020

Ionic liquid induced controllable synthesis of nickel-hydroxide-encapsulated NiFe layered double hydroxide for efficient oxygen evolution

Wenqiang Wu[1,2], Kaihang Yue[2], Kang Zhang[2], Jingcheng Xu[1], Xia Bao Yu[3*], Yan Ya[2*] and Xianying Wang[2*]

The efficiency of electrochemical water splitting is severely restricted by the slow oxygen evolution reaction (OER) on the anode. Therefore, the design and synthesis of high-performance electrocatalysts for anodic oxygen evolution is crucial for the industrialization of hydrogen production by electrolysis of water. Herein, an efficient core-shell $Ni(OH)_2$@NiFe LDH electrocatalyst was designed with the assistant of ionic liquid for OER. The ionic liquid delayed the crystallization ability of Ni^{2+} ions and then facilitated the formation of NiFe LDH coated $Ni(OH)_2$ structure. The as-obtained core-shell $Ni(OH)_2$@NiFe LDH exhibited outstanding OER electrocatalytic activity that only required overpotentials of 258 mV to deliver current densities of 100 mA cm^{-2}, and a decent stability of at least 300 h under a large current density of 100 mA cm^{-2}. This study provides a valuable reference for the structure design of NiFe LDH based catalyst.

The extensive use of fossil fuels has led to a range of energy and environmental problems, which forces the development of new renewable energy sources to be imminent[1]. Electrocatalytic water splitting to produce hydrogen is one of the research hotspots in seeking new energy sources[2,3]. It consists of two half-reactions: hydrogen evolution reaction (HER) and oxygen evolution reaction (OER)[4,5]. However, the slow OER reaction involves four electron coupling processes, which seriously affects the overall water decomposition efficiency. Precious metal based materials (Such as IrO_2 and RuO_2) have been selected as benchmark electrocatalysts for OER because of their good catalytic activity and stability in acidic environments[6,7]. Unfortunately, their rarity and cost limit their wide application. Therefore, it is important to explore efficient non-noble metal catalysts to replace noble metal-based catalysts.

Layered double hydroxides (LDHs) are known as a type of the most excellent alkaline OER catalysts owing to their outstanding activity and stability[8,9]. Unfortunately, the limited active sites in traditional NiFe LDH and its poor conductivity cannot live up to the expectation[10–12]. So far, various physicochemical strategies have been implemented to modulate the electrochemistry OER performance of LDH such as core-shell nanostructure and engineering defects[13,14]. And great success has been achieved in the electrocatalytic applications of core-shell structured LDHs. For instance, Cai et al. developed three-dimensional porous core-shell NiFe/Ni NCs layered double hydroxide nanosheets with extraordinary OER[15]. The inner Ni metallic cores could serve as the highly conductive layer to facilitate reliable electron transfer and to improve the electrical conductivity of NiFe LDH. Feng et al. designed a cactus-like $NiCo_2S_4$@NiFe LDH core-shell hollow sphere assembled by one-dimensional NiFe LDH nanowires and two-dimensional NiFe LDH nanosheets on the $NiCo_2S_4$ hollow spheres[16]. The integration of NiFe LDH into $NiCo_2S_4$ to form core-shell structure and the strong electronic interaction between NiFe LDH and $NiCo_2S_4$ can greatly improve OER activity, and the external NiFe LDH nanowires and NiFe LDH nanosheets can effectively inhibit the collapse and corrosion of the internal $NiCo_2S_4$ hollow structure. However, these well-designed core-shell structures usually involves multi-step synthesis process, which leads to a complicated process and is difficult to meet the actual requirements. Therefore, it is desirable to develop a simple and efficient method to synthesize NiFe LDH based core-shell structure with enhanced OER performance.

Ionic liquid (IL) is a widely used solvent and template to synthesize inorganic materials due to its low surface tension, good integration with other phases, long hydrophobic group, high conductivity polarity, and high thermal stability[17,18]. In light of these special properties and the composition, herein, a N, B, F-containing ionic liquid (1-Butyl-3-Methylimidazolium Tetrafluoroborate, $BMIMBF_4$) was selected to synthesize the NiFe LDH-based hybrid structure. Owing to the different ion diffusion and crystallization rate induced by the ionic liquid, a

[1] *School of Materials and Chemistry, University of Shanghai for Science and Technology, 516 Jungong Road, Shanghai 200093, China*

[2] *CAS Key Laboratory of Materials for Energy Conversion, Shanghai Institute of Ceramics, Chinese Academy of Sciences (SICCAS), 585 Heshuo Road, Shanghai 200050, China*

[3] *School of Chemistry and Chemical Engineering, Key Laboratory of Material Chemistry for Energy Conversion and Storage (Ministry of Education), Huazhong University of Science and Technology (HUST), 1037 Luoyu Rd, Wuhan 430074, China*

* Corresponding author, E-mail: byxia@hust.edu.cn; yanya@mail.sic.ac.cn; wangxianying@mail.sic.ac.cn

Received 24 December 2022; Accepted 10 March 2023; Published online

DOI: 10.54227/elab.20220020

core-shell structure with NiFe LDH coated $Ni(OH)_2$ ($Ni(OH)_2$@NiFe LDH) was designed by a simple one-step hydrothermal method. The obtained $Ni(OH)_2$@NiFe LDH electrocatalyst showed much better OER performance than pure NiFe LDH as well as an excellent cell performance when assembled in an anion exchange membrane electrolyzer. This work opens a simple method for the synthesis of efficient and durable hydroxide electrocatalysts using ionic liquids as dopants and templates and is a promising candidate strategy for the preparation of other electrocatalysts.

Materials and methods

Chemicals and reagents

The chemicals were used as received without further purification. Hydrochloric acid (HCl, AR, Adamas, Shanghai, P.R. China), ethanol (C_2H_6O, ≥ 99.7 %, Adamas, Shanghai, P.R. China), Nickel (II) nitrate hexahydrate ($Ni(NO_3)_2{\cdot}6H_2O$, 98%, Aladdin Co., P.R. China), Ferric (III) nitrate nonahydrate ($Fe(NO_3)_3{\cdot}9H_2O$, 99.95 %, Aladdin Co., P.R. China), urea ($CO(NH_2)_2$, 99%, Aladdin Co., P.R. China), 1-Butyl-3-Methylimidazolium Tetrafluoroborate ($C_8H_{15}BF_4N_2$, 99%, Adamas, Shanghai, P.R. China), Nafion D-521 solution (5 %, Alfa Aesar), Iridium (IV) Oxide (IrO_2, 99.9 %, Adamas, Shanghai, P.R. China), Potassium hydroxide (KOH, ACS, Aladdin Co., P.R. China), and Ni foam (1.0 mm in thickness, the surface area of ~1.9 $m^2\ g^{-1}$, Tianjin EVS Co., P.R. China). Deionized (DI) water with a resistance of ~18.2 MΩ was used throughout all experiments.

Synthesis of $Ni(OH)_2$@NiFe LDH catalyst

In a typical synthesis, Ni foam (NF) was ultrasonically cleaned with 3.0 M hydrochloric acid for 15 min to effectively remove the surface nickel oxides, and subsequently rinsed with deionized water and ethanol several times and dried at 60 °C for 10 min. Then, 261 mg Ni $(NO_3)_2{\cdot}6H_2O$, 40 mg Fe $(NO_3)_3{\cdot}9H_2O$, and 300 mg urea were dissolved into deionized water (30 mL) with continuous magnetic stirring for 0.5 h at room temperature, and a yellow, transparent, and homogeneous solution was obtained in the reaction cell. 120 mg of ionic liquid (1-Butyl-3-methylimidazolium tetrafluoroborate, BMIMBF4) was injected into the above-mixed solution and stirred for 1 h. The as-obtained homogeneous solution was transferred into a 50 mL autoclave in the presence of the as-treated NF, sealed, and heated in an oven at 120 °C for 12 h. Subsequently, after the autoclave cooled down to room temperature, the sample was collected and washed thoroughly with distilled water and absolute ethanol several times, and then dried at 60 °C for 6 h in the oven. For comparison, NiFe LDH was deposited on NF by using the same synthetic method without ionic liquid, denoted as NiFe LDH.

Materials characterization

The morphology and structure of the as-synthesized samples were detected with scanning electron microscopy (SEM, LEO 1530VP), transmission electron microscope (TEM, FEI Tecnai G2 F20 S-TWIN) coupled with energy dispersive X-ray spectroscopy (EDX), HAADF-STEM analyses (JEOL JEM-ARM200F S/TEM with a spherical aberration corrector). The elemental composition was investigated with Inductively Coupled Plasma Optical Emission Spectrometry (ICP-OES, Thermo Fisher iCAP PRO). The phase composition and chemical bonding nature in the samples were characterized by Fourier Transform infrared spectroscopy (FTIR, Thermo Nicolet NEXUS 470). Surface chemical compositions of the samples were characterized by an X-ray photoelectron spectroscopy (XPS, AXIS ultra DLD, Shimazu) in a vacuum of 10-7 Pa with an Al Kα monochrome anode.

Electrochemical measurement

All electrochemical performance of the catalyst was performed on a GAMRY workstation at room temperature. The electrolyze cell of three electrodes was used for all experiments while using the catalysts on NF as the working electrode, the graphite rod electrode served as the counter electrode, and Hg/HgO as the reference electrode. 1 M KOH was employed as the electrolyte solution. All potentials in this article are measured relative to Hg/HgO, but they were relative to the reversible hydrogen electrode (RHE) and are determined by $E_{RHE} = E_{Hg/HgO} + 0.098 + 0.059 \times pH$. Cycle voltammetry (CV) of the OER test was performed from 0 V to 1 V vs. Hg/HgO at a scan rate of 5 mV s^{-1}, and the electrochemical impedance spectroscopy (EIS) was measured in the frequency range of 0.01 Hz to 100 kHz. In addition, tested the CV curve at different scanning speeds, which are employed to estimate the double-layer capacitances (C_{dl}) of the catalysts. The long stability of catalysts was also tested by chronopotentiometry, which was carried out at a constant overpotential of 100 mA cm^{-2} for 300 h.

The Faraday efficiency is obtained by collecting gas by draining water. The average evolution rates of H_2 and O_2 can be obtained based on the generated gas amount in unit electrolysis time. The Faraday efficiency (FE) value was obtained by the following equations:

$$FE = z \times n \times F/(I \times t) \times 100\%$$

$$n = PV/RT$$

where z is the electron transfer number, n is the amount (moles) of the generated gas in the experiment, F is the Faraday constant (96,485.3 C mol^{-1}), I is the applied constant current (A), t is the electrolysis time (s), P is the pressure (pa), V is the gas volume, R is the molar gas constant (8.31), and T is the gas temperature (K).

Alkaline anion exchange membrane water electrolysis (AEMWE) test

The AEMWE system consists of the anode, cathode, gas diffusion layer, and anion exchange membrane (AEM, X37-50 Grade T, Dioxide Materials). The direct-grown $Ni(OH)_2$@NiFe LDH on Ni foam (thickness: 0.15 mm) was used as an anode electrode. The cathode electrode was prepared by the catalyst-coated substrate method. The NiFe LDH/Ni NCs were used as the electrode for the hydrogen evolution reaction (HER) on Ni foam. The fastening pressure of the AEMWE cell is 20 N/m at each of the 8 bolts. The performance of an AEMWE with an active area of 1 cm × 1 cm was evaluated through CV in the range of 1.0 to 2.0 V cells at a scan rate of 5 mV s^{-1} and stability test at different current densities (0.5 A, 1.0 A, 1.5 A, and 2.0 A) in 1 M KOH at 25 °C

Results and Discussion

The synthetic strategies for the $Ni(OH)_2$@NiFe LDH involved the following steps and are schematically exhibited in

DOI: 10.54227/elab.20220020

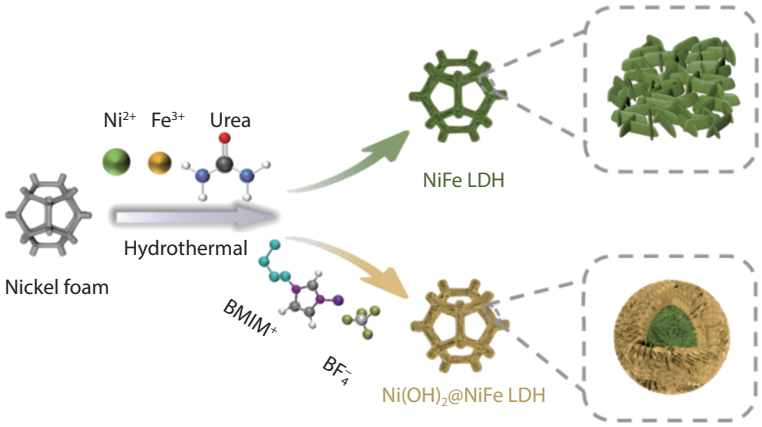

Fig. 1 Schematic illustration of the formation and transform the process of $Ni(OH)_2$@NiFe LDH.

Figure 1. Without the presence of ionic liquid, a nanosheet-structured NiFe-LDH with serious adhesion and agglomeration was obtained (Figure S1a-c). Interestingly, when ionic liquid is added, a core-shell structure with $Ni(OH)_2$ coated NiFe LDH yields. The representative scanning electron microscopy (SEM) and transmission electron microscopy (TEM) images of the $Ni(OH)_2$@NiFe LDH indicate that amounts of uniform nanospheres composed of ultrathin nanosheets are observed (Figure 2a-c). The high-resolution TEM image (Figure 2d) reveals that $Ni(OH)_2$@NiFe LDH displays a lattice spacing of about 0.235 nm, which corresponds to the (011) crystal plane of $Ni(OH)_2$. Similarly, this result is also confirmed by the selected area electron diffraction (SAED) pattern of $Ni(OH)_2$@NiFe LDH (Figure 2d inset). It displays two clear diffraction rings with radiuses of 0.154 nm and 0.237 nm, respectively, corresponding to the (110) crystal plane in NiFe LDH and the (011) crystal plane in $Ni(OH)_2$. Detailed element semi-quantitative information studies are performed to confirm the core-shell structure and the images shown in Figure 2e-l. Line scanning profiles and energy-dispersive spectroscopy (EDS) elemental mapping demonstrates the distribution of Ni, Fe, O, N, B, and F elements throughout the whole nanostructure. Interestingly, the Fe element in $Ni(OH)_2$@NiFe LDH is concentrated in the center of the nanosphere, while the Ni content in the center area is obviously less than that in the edge area. As a comparison, the Ni and Fe elements in NiFe LDH are distributed very evenly (Figure S1d-i). Therefore, it can be preliminarily judged that ionic liquid induced the formation of this core-shell structure. Besides, the observation of N, B, and F in the sample could be due to the degradation of BMIM cations, which releases N atoms and lead to the formation of N element doping, while the BF_4^- anionic substance may be hydrolyzed into $[BF_3OH]$ and HF, which results in the doping of elements B and F[19].

According to the research on the ion liquids[20], the $[BF_4^-]$ would interact with Ni atoms to form the Ni-BF_4 species after introducing $[Bmim][BF_4]$ in the hydrothermal process. As the Ni-BF_4 interaction bonds possess an activation barrier of 1.15 eV, 3 times higher than that without $[Bmim][BF_4]$[21], which would decease the formation rate of Ni based oxides. To verify the formation mechanism of $Ni(OH)_2$@NiFe LDH, the contents of Ni and Fe elements remaining in the solution after different hydrothermal reaction times were measured. With the aid of inductively coupled plasma optical emission spectrometry (ICP-OES) testing (Table. S1), it is found that the crystallization rate of Ni^{2+} ions obviously slows down when ionic liquid is added. In addition, the distribution trend of N and F elements belonging to ionic liquids is similar to that of Ni elements, this further indicates that there is interaction between ionic liquids and Ni^{2+}ions. Based on the above experimental results and analysis, we suspect this core-shell structure can be attributed to that the ionic liquid inhibits the crystallization rate of Ni^{2+} ions, so that NiFe LDH with a higher Fe/Ni atomic ratio preferentially grows to form nuclei, and then the remaining Ni^{2+} ions continue to crystallize and grow to form $Ni(OH)_2$ shell[22,23]. Moreover, the effect of different concentrations of $BMIMBF_4$ on the structure was investigated. The results showed that with the increase of ionic liquid concentration, the adhesion between nanosheets decreased, but when ionic liquid was excessive, nanosheets became thicker and the nanosphere shapes were damaged. (Figure S2). In addition, no core-shell structure was observed when synthesis CoFe-LDH with same method (Figure S3), which shows that $BMIMBF_4$ modifies LDH to make it have a core-shell structure that is not universal. The core-shell structure in this work depends on the interaction of Ni^{2+} ions, Fe^{3+} ions, and ionic liquids.

The X-ray diffraction (XRD) is performed to further confirm the phase of this core-shell structure (Figure 3a). Besides of the obvious diffraction peaks at 44.51° and 51.84° for nickel foam (NF). The characteristic diffraction peak of the catalyst on nickel foam is very weak. To clearly judge the phase of the catalyst, powder samples were used for further characterization (Figure S4). Obviously, these diffraction peaks can be well matched with NiFe LDH (JCPDS#040-0215) phase and $Ni(OH)_2$ (JCPDS#074-2075) phase, indicating that there are two phases in the catalyst. Combined with the results of TEM line scanning, it is clear that the catalyst has a core-shell structure $Ni(OH)_2$@NiFe LDH[24,25]. The Raman spectrum of $Ni(OH)_2$@NiFe LDH displays three characteristic peaks at 452 cm^{-1}, 527 cm^{-1}, and 712 cm^{-1} for LDH (Figure 3b)[26]. In addition, a weak peak at 1045 cm^{-1} is associated with carbonate ions in the interlayer of the LDH[27], while another peak at 310 cm^{-1} associated with Ni-O vibrations of the β-$Ni(OH)_2$, which further proved the formation of $Ni(OH)_2$[28]. The N_2 adsorption/desorption isotherm in Figure S5 shows the characteristics of

DOI: 10.54227/elab.20220020

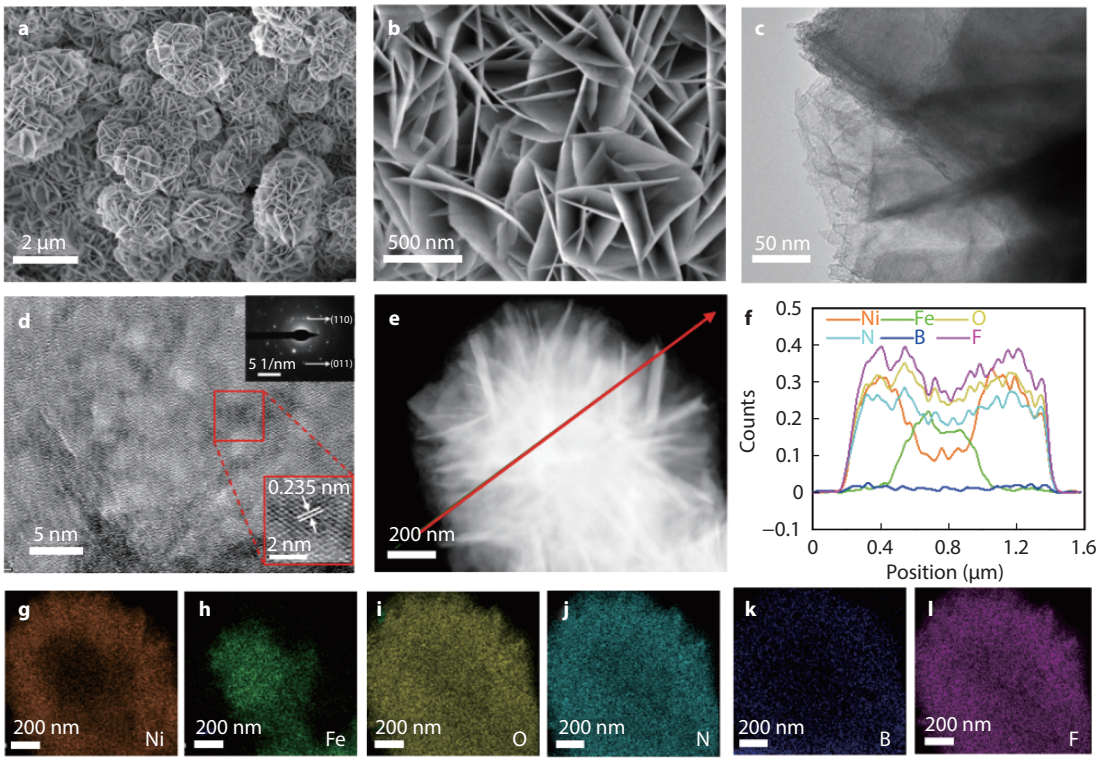

Fig. 2 **a-b** SEM images, **c** TEM image, **d** HRTEM (inset shows the corresponding SAED pattern), and **e** HAADF-STEM, **f** line scanning profiles of Ni, Fe, O, N, B, and F recorded along the line shown in **e**, and **g-l** element mapping of the $Ni(OH)_2$@NiFe LDH.

micropores and mesopores. The rapid adsorption and pickup at low pressure represent micropores, while the appearance of a hysteresis loop indicates that mesopores exist in $Ni(OH)_2$@NiFe LDH. The Brunauer-Emmett-Teller (BET) surface area and pore volume of $Ni(OH)_2$@NiFe LDH are calculated as 40.22 $m^2\ g^{-1}$ and 0.129 $cm^3\ g^{-1}$. Further FTIR spectrum of the $Ni(OH)_2$@NiFe LDH shows that the bands at around 600 cm^{-1} are related to the metal-oxygen-metal lattice vibrations of the layer cations of NiFe LDH (Figure 3c)[29,30]. The stretching modes of the hydroxyl groups, bending modes of free water molecules, and antisymmetric stretching vibration of nitrate anions are confirmed at 3400-3600 cm^{-1}, 1636.3 cm^{-1}, and 1384.2 cm^{-1}, respectively[31–33].

X-ray photoelectron spectroscopy (XPS) measurements are also performed to investigate and study the surface elemental composition as well as the chemical states of the catalyst. The XPS survey spectrum indicates the coexistence of Ni, Fe, O, N, B, and F elements (Figure S6), which is in good agreement with the elemental mapping result. As for the Ni 2p spectra of $Ni(OH)_2$@NiFe LDH and NiFe LDH, the binding energies at 856.3 eV and 874.0 eV along with their shake-up satellites peaks at 861.7 eV and 880.0 eV are attributed to Ni $2p_{3/2}$ and Ni $2p_{1/2}$, respectively (Figure 3d), the additional Ni^0 peak at 852.02 eV can be assigned to NF substrates[34]. Figure 3e shows that the Fe $2p_{3/2}$ peaks at 710 eV and 714.20 eV confirm the presence of the Fe^{2+} and Fe^{3+} oxidation states, respectively[35]. In O 1s fine spectra (Fig. 3f), there are three types of O species on these materials, which are assigned to lattice oxygen atoms bound to Ni or Fe with lower binding energy (531.1 eV for M-O-H), oxygen vacancies or defective oxygen with low coordination at medium binding energy (531.8 eV for V_O), and surface-adsorbed oxygen with higher binding energy (533 eV for H-O-H)[13,16,36]. Apparently, $Ni(OH)_2$@NiFe LDH shows more hydroxide species than pure NiFe LDH. The N 1s spectra of the $Ni(OH)_2$@NiFe LDH catalyst is shown in Figure 3g to determine the possible metal-N interactions. In the $Ni(OH)_2$@NiFe LDH hybrid, three different types of nitrogen species at 398.5 eV (N1), 399.8 eV (N2), and 401.4 eV (N3) are attributed to the metal-N bond, pyridinic N, and pyrrolic N respectively[37,38]. In Figure 3h, the B 1s spectra for $Ni(OH)_2$@NiFe LDH showed the formation of a boron peak[39]. The F 1s peak with a binding energy of 686.2 eV for the $Ni(OH)_2$@NiFe LDH catalyst was attributed to the M-F species (Figure 3i)[40].

The oxygen evolution activity of the prepared catalysts was evaluated in a three-electrode system under 1 M KOH electrolyte. The core-shell nanostructure $Ni(OH)_2$@NiFe LDH was used directly as the working electrode. For comparison, the electrocatalytic activity of $Ni(OH)_2$-NiFe LDH (prepared by electrodeposition $Ni(OH)_2$ on the surface of NiFe LDH, Figure S7), NiFe LDH, $Ni(OH)_2$, and IrO_2 were also measured. As seen from the linear sweep voltammetry (LSV) curves in Figure 4a and Figure S8, the $Ni(OH)_2$@NiFe LDH requires an overpotential of only 258 mV to achieve the current density of 100 mA cm^{-2}, much lower than that of $Ni(OH)_2$, (463 mV)and IrO_2 (385 mV), and even better than those of $Ni(OH)_2$-NiFe LDH (297 mV) and NiFe LDH (310 mV). This fully shows the advantage of the N, B, F doped $Ni(OH)_2$@NiFe LDH core-shell structure induced by ionic liquid for oxygen evolution. The catalysts that prepared with different amounts of ionic liquid were also tested. It is found that the $Ni(OH)_2$@NiFe LDH prepared with 120 mg ionic liquid has the best OER performance (Figure S9).

DOI: 10.54227/elab.20220020

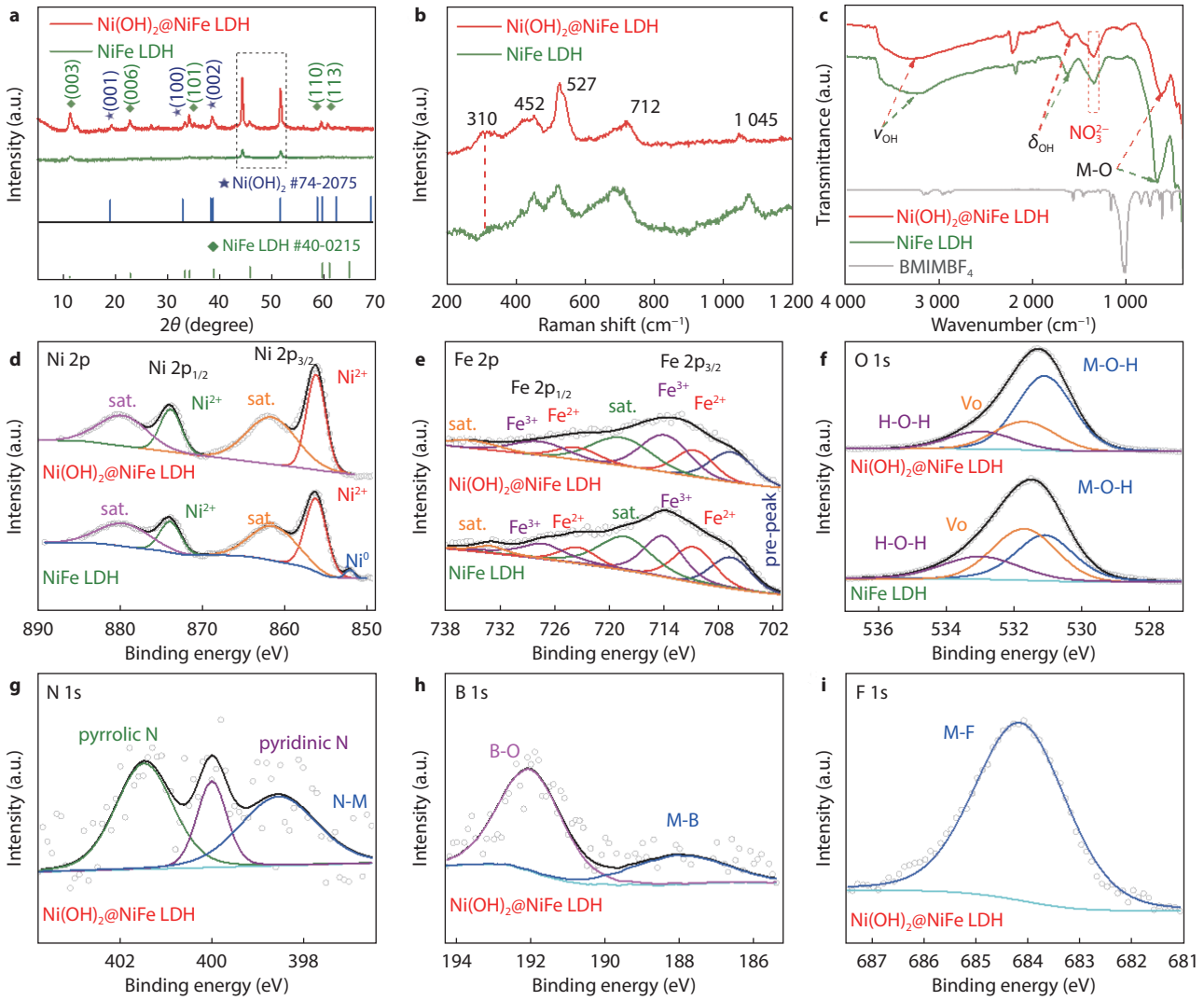

Fig. 3 **a** XRD patterns, **b** Raman spectra of the $Ni(OH)_2$@NiFe LDH and NiFe LDH. **c** FT-IR spectra of $Ni(OH)_2$@NiFe LDH, NiFe LDH, and $BMIMBF_4$. XPS spectra for $Ni(OH)_2$@NiFe LDH and NiFe LDH **d** Ni 2p, e Fe 2p, f O 1s, g N 1s, h B 1s, i F 1s.

In addition, the Tafel slope of $Ni(OH)_2$@NiFe LDH (42.94 mV dec^{-1}) is inherently better than that of $Ni(OH)_2$-NiFe LDH (74.52 mV dec^{-1}) and NiFe LDH (52.83 mV dec^{-1}), demonstrating its intrinsically favorable activity and kinetics (Figure 4b). This may be due to the synergistic effect between NiFe LDH, $Ni(OH)_2$ and the doped N, B, F elements, which offers the rapid mass transfer and optimized electronic structure of the metal active sites. To verify the relationship between OER performance and doping N, B, and F elements, we used different ionic liquids to modify the catalyst. The catalyst modified by $BMIMBF_4$ has the best OER performance (Figure S10), while the 1-butyl-3-methylimidazolium nitrate ($BMIMNO_3$) and 1-butyl-3-methylimidazolium hexafluorophosphate ($BMIMPF_6$) have a negative effect on the catalytic activity of NiFe LDH. Further SEM images shows that the NiFe LDH modified with $BMIMNO_3$ or $BMIMPF_6$ yielded a bonded and agglomerated nanostructure and thus decreased catalytic active sites (Figure S11). To further deepen the insights into the OER performance evaluation, a detailed comparison with recently reported OER catalysts is given in Table S2. In these cases, we can evidently conclude that the $Ni(OH)_2$@NiFe LDH affords an extraordinary OER performance, outperforming many state-of-the-art noble metal-free OER catalysts in alkaline medium. The electrochemical impedance spectroscopy (EIS) was also performed (Figure 4c), and the diameter of the semicircle is related to the charge transfer resistance (R_{ct}). It can be seen that $Ni(OH)_2$@NiFe LDH exhibits the smallest R_{ct} in comparison to other catalysts, indicating the fast OER kinetics that occurred on the surface of $Ni(OH)_2$@NiFe LDH. Furthermore, electrochemical active surface area (ECSA) is another factor to access the OER activity, which is determined by the double-layer capacitance (C_{dl}) resulting from Cycle voltammetry (CV) curves in the non-Faradic region (Figure S12). As shown in Figure 4d, the C_{dl} value of $Ni(OH)_2$@NiFe LDH (2.09 mF cm^{-2}) is higher than that of pure NiFe LDH (1.48 mF cm^{-2}), revealing that the introduction of the ionic liquid can increase the electrochemically active area and expose more active sites, thus boost the OER activity. The intrinsic electrocatalytic activity of different catalysts was evaluated using ECSA-normalized LSV curves (Figure S13), which indicated that the

DOI: 10.54227/elab.20220020

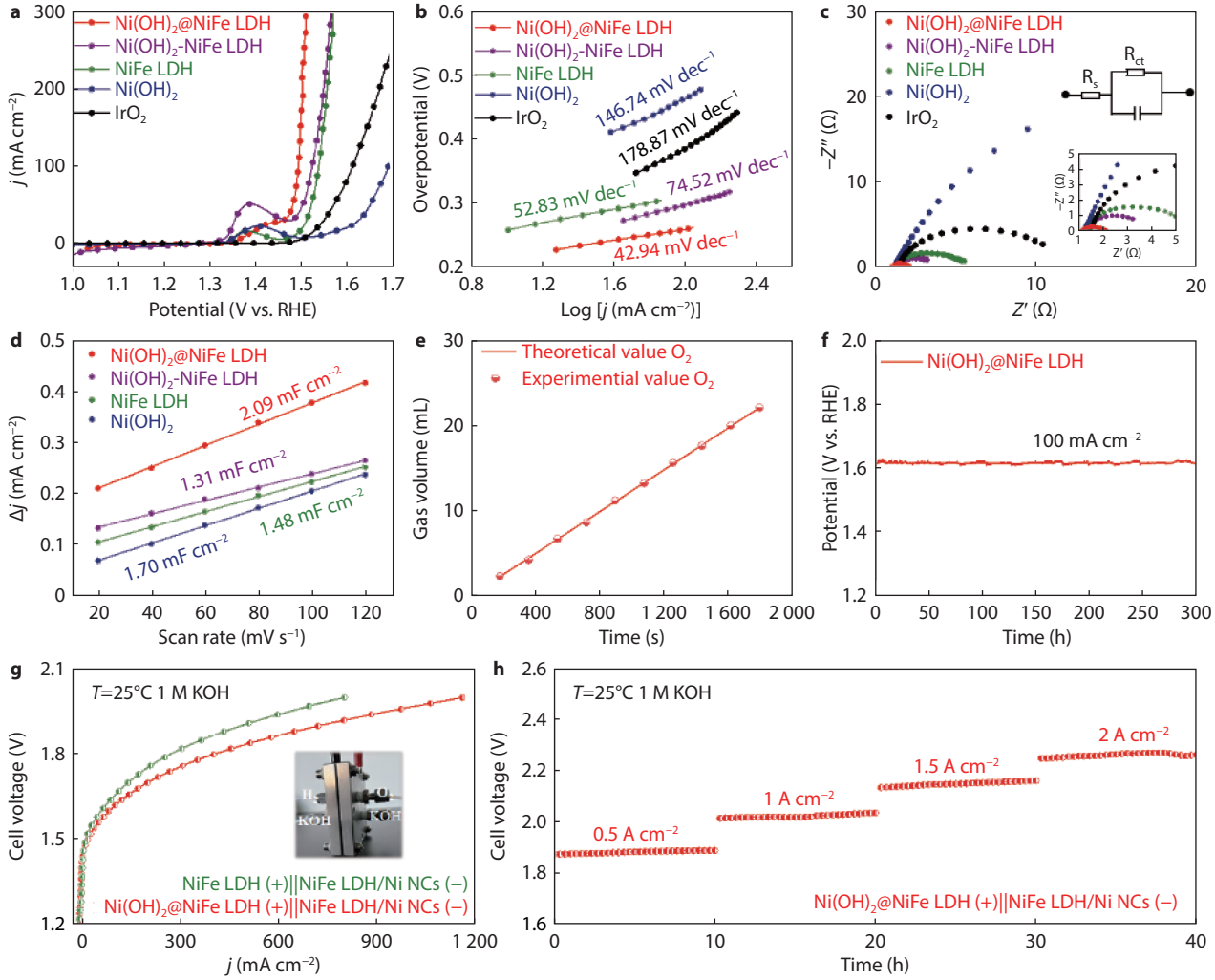

Fig. 4 **a** LSV curves, **b** Tafel slopes, **c** Nyquist plots (inset: equivalent circuit model), **d** C_{dl} values, and **e** The amount of H_2 and O_2 catalyzed by the $Ni(OH)_2$@NiFe LDH || NiFe LDH/Ni NCs **f** Chronoamperometric curves for the OER. **g** Polarization curves of the AEMWE cell using $Ni(OH)_2$@NiFe LDH || NiFe LDH/Ni NCs on Ni foam (inset: the AEMWE cell photograph). **h** The durability of the AEMWE cell at different current densities.

$Ni(OH)_2$@NiFe LDH has the best intrinsic catalytic activity. It can be seen that $Ni(OH)_2$@NiFe LDH has a larger electrocatalytic active area compared with NiFe LDH nanosheet and $Ni(OH)_2$ nanosheet, which is also an important reason for the improvement of its electrocatalytic oxygen evolution performance. This result is consistent with the trend of OER activity (Figure 4a). To detect the oxygen evolution efficiency of $Ni(OH)_2$@NiFe LDH, the faraday efficiency was calculated by collecting hydrogen and oxygen with a double electrode system. Figure 4e shows that the evolution rate of oxygen is 12.27 μl s^{-1}, corresponding to a faraday efficiency of 99.85%. In addition, durability is another index to estimate the performance of the catalyst. In addition, durability is another index to evaluate the performance of catalyst. As displayed in Figure 4f and Figure S14, the NiFe LDH shows strong stability than the $Ni(OH)_2$ catalyst. Benefiting from the merits of core NiFe LDH, the $Ni(OH)_2$@NiFe LDH has a relatively constant operating potential without significant degradation over 300 h. Related characterization of $Ni(OH)_2$@NiFe LDH after the stability test demonstrated that both the structure and the chemical state of the elementals maintained well (Figure S15-S17), all these factors make great contribution to the excellent durability performance.

Furthermore, the prepared catalyst was assembled into an alkaline anion exchange membrane (AEM) electrolyzer (Figure 4g inset) as the anode catalyst, and the cathode catalyst was NiFe LDH/Ni NCs (NiFe LDH/Ni NCs is prepared as our previous report[15]). The linear scanning curves of the AEM cell were performed at 25 °C in 1 M KOH (Figure 4g), The $Ni(OH)_2$@NiFe LDH || NiFe LDH/Ni NCs electrolyzer cell delivered a high current density of j = 1 A cm^{-2} at a cell voltage of 2 V, which is far better than NiFe LDH || NiFe LDH/Ni NCs catalysts (j = 0.8 A cm^{-2} at 2 V). The catalytic stability of the assembled AEMWE cell was tested by applying different constant current densities with a total measurement time of 40 h (Figure 4h), the results illustrate that $Ni(OH)_2$@NiFe LDH assembled cell displayed excellent stability at different current density. The above observation suggests the potential application of such catalysts toward commercial water electrolysis,

DOI: 10.54227/elab.20220020

Conclusions

In summary, a core-shell $Ni(OH)_2$@NiFe LDH catalyst with NiFe LDH as the core and $Ni(OH)_2$ as the shell was successfully designed with the aid of ionic liquid. During this process, the crystallization rate of Ni^{2+} ions is suppressed, which leads to the preferential depletion of Fe^{3+} ions to form NiFe LDH, and then the excess Ni^{2+} ions continue to grow on NiFe LDH surface to obtain $Ni(OH)_2$@NiFe LDH with core-shell structure. Owing to the unique structure resulted large surface area, highly exposed active sites, and synergistic coupling effects among electrocatalytically active species, the as-obtained $Ni(OH)_2$@NiFe LDH doped with N, B, F exhibits superior OER activity with a low overpotential of 258 mV to reach a current density of 100 mA cm^{-2} and a small Tafel slope of 42.94 mV dec^{-1}. Moreover, the $Ni(OH)_2$@NiFe LDH displays a stable oxygen output at a high current density of 100 mA cm^{-2}. This study provides a facile method for the synthesis of highly efficient and durable NiFe electrocatalysts for water oxidation technology.

■ ACKNOWLEDGMENTS

This project is funded by financial support from the National Natural Science Foundation of China (22279159), Natural Science Foundation of Shanghai (22ZR1471900), and Shanghai Rising-Star Program (22QA1410300). We also acknowledge the financial support by the Shanghai Municipal Science and Technology Commission of Carbon Peak & Carbon Neutrality Project (21DZ1207900).

■ SUPPORTING INFORMATION

Additional results for material characterizations and electrochemical measurements, and comparisons of the performance

■ CONFLICT OF INTEREST

The authors declare no conflict of interest.

■ AUTHOR CONTRIBUTIONS

Yan Ya, Xianying Wang proposed the research direction and guided the project; Wenqiang Wu, Kaihang Yue and Kang Zhang performed the experiments; Wenqiang Wu, Jingcheng Xu and Yan Ya analyzed and discussed the experimental results; Wenqiang Wu, Xia Bao Yu and Yan Ya drafted the manuscript. All authors joined the discussion of data and approved the final version.

■ REFERENCES

1. Y. Yan, J.-Y. Zhang, X.-R. Shi, Y. Zhu, C. Xia, S. Zaman, X. Hu, X. Wang and B. Y. Xia, *ACS Nano*, 2021, 15, 10286
2. Y. Zhu, K. Yue, C. Xia, S. Zaman, H. Yang, X. Wang, Y. Yan and B. Y. Xia, *Nano-Micro Lett.*, 2021, 13, 137
3. Y. Yan, Y. Xu, B. Zhao, Y. Xu, Y. Gao, G. Chen, W. Wang and B. Y. Xia, *J. Mater. Chem. A*, 2020, 8, 5070
4. R. Gao and D. Yan, *Nano Res.*, 2018, 11, 1883
5. Z. Guo, W. Ye, X. Fang, J. Wan, Y. Ye, Y. Dong, D. Cao and D. Yan, *Inorg. Chem. Front.*, 2019, 6, 687
6. T. Binninger and M.-L. Doublet, *Energy Environ. Sci.*, 2022, 15, 2519
7. J. Wang, C. Cheng, Q. Yuan, H. Yang, F. Meng, Q. Zhang, L. Gu, J. Cao, L. Li, S.-C. Haw, Q. Shao, L. Zhang, T. Cheng, F. Jiao and X. Huang, *Chem*, 2022, 8, 1673
8. R. Gao and D. Yan, *Adv. Energy Mater.*, 2020, 10, 1900954
9. L. Zhang, J. Han, R. Wang, X. Qiu, and J. Ji, *J. Chem. Eng. Data*, 2007, 52, 1401
10. R. Chen, S.-F. Hung, D. Zhou, J. Gao, C. Yang, H. Tao, H. B. Yang, L. Zhang, L. Zhang, Q. Xiong, H. M. Chen and B. Liu, *Adv. Mater.*, 2019, 31, 1903909
11. R. Gao, J. Zhu and D. Yan, *Nanoscale*, 2021, 13, 13593
12. L. Zhou, C. Zhang, Y. Zhang, Z. Li and M. Shao, *Adv. Funct. Mater.*, 2021, 31, 2009743
13. Z. Cai, P. Wang, J. Zhang, A. Chen, J. Zhang, Y. Yan and X. Wang, *Adv. Mater.*, 2022, 34, 2110696
14. L. Peng, N. Yang, Y. Yang, Q. Wang, X. Xie, D. Sun-Waterhouse, L. Shang, T. Zhang and G. I. N. Waterhouse, *Angew. Chem. Int. Ed.*, 2021, 60, 24612
15. Z. Cai, X. Bu, P. Wang, W. Su, R. Wei, J. C. Ho, J. Yang and X. Wang, *J. Mater. Chem. A*, 2019, 7, 21722
16. X. Feng, Q. Jiao, W. Chen, Y. Dang, Z. Dai, S. L. Suib, J. Zhang, Y. Zhao, H. Li and C. Feng, *Appl. Catal. B*, 2021, 286, 119869
17. M. V. Fedorov and A. A. Kornyshev, *Chem. Rev.*, 2014, 114, 2978
18. J. Sun, N. Guo, Z. Shao, K. Huang, Y. Li, F. He and Q. Wang, *Adv. Energy Mater.*, 2018, 8, 1800980
19. B. Murugesan, N. Pandiyan, M. Arumugam, M. Veerasingam, J. Sonamuthu, A. R. Jeyaraman, S. Samayanan and S. Mahalingam, *Carbon*, 2019, 151, 53
20. J. Dupont and J. D. Scholten, *Chem. Soc. Rev.*, 2010, 39, 1780
21. L. Fan, L. Zhao, Y. Lv, T. Wang, Y. Tian, J. Fu and X. Liu, *Inorg. Chem. Front.*, 2022, 9, 3679
22. J. Hong, T. T. Mengesha, S.-W. Hong, H.-K. Kim and Y.-H. Hwang, *J. Korean Phys. Soc.*, 2020, 76, 264
23. C. Y. Xu and Y. X. Hua, *Mater. Sci. Forum*, 2011, 633, 1163
24. C. Li, Z. Zhang and R. Liu, *Small*, 2020, 16, 2003777
25. Y. Yan, G. Cheng, P. Wang, D. He and R. Chen, *RSC Adv.*, 2014, 4, 49303
26. Y. Zhai, X. Ren, Y. Sun, D. Li, B. Wang and S. Liu, *Appl. Catal. B*, 2023, 323, 122091
27. J. Zhang, A. Wei, J. Liu, J. Zhu, Y. He and Z. Liu, *J. Alloys Compd.*, 2022, 927, 166990
28. T. u. Haq, Y. Haik, I. Hussain, H. u. Rehman and T. A. Al-Ansari, *ACS Appl. Mater. Interfaces*, 2021, 13, 468
29. X. Ge, C. Gu, Z. Yin, X. Wang, J. Tu and J. Li, *Nano Energy*, 2016, 20, 185
30. J.-J. Lv, J. Zhao, H. Fang, L.-P. Jiang, L.-L. Li, J. Ma and J.-J. Zhu, *Small*, 2017, 13, 1700264
31. J. L. Gunjakar, B. Hou, A. I. Inamdar, S. M. Pawar, A. T. A. Ahmed, H. S. Chavan, J. Kim, S. Cho, S. Lee, Y. Jo, S.-J. Hwang, T. G. Kim, S. Cha, H. Kim and H. Im, *Small*, 2018, 14, 1703481
32. Y. Hou, M. R. Lohe, J. Zhang, S. Liu, X. Zhuang and X. Feng, *Energy Environ. Sci.*, 2016, 9, 478
33. M.-F. Chiang and T.-M. Wu, *Appl. Clay Sci.*, 2011, 51, 330
34. K. Yue, J. Liu, Y. Zhu, C. Xia, P. Wang, J. Zhang, Y. Kong, X. Wang, Y. Yan and B. Y. Xia, *Energy Environ. Sci.*, 2021, 14, 6546
35. K. Yue, J. Liu, C. Xia, K. Zhan, P. Wang, X. Wang, Y. Yan and B. Y. Xia, *Mater. Chem. Front.*, 2021, 5, 7191
36. Y. Zhu, L. Zhang, B. Zhao, H. Chen, X. Liu, R. Zhao, X. Wang, J. Liu, Y. Chen and M. Liu, *Adv. Funct. Mater.*, 2019, 29, 1901783

DOI: 10.54227/elab.20220020

37. J. Yang, X. Wang, B. Li, L. Ma, L. Shi, Y. Xiong and H. Xu, *Adv. Funct. Mater.*, 2017, 27, 1606497
38. C. Hu and L. Dai, *Adv. Mater.*, 2017, 29, 1604942
39. I.-K. Ahn, S.-Y. Lee, H. G. Kim, G.-B. Lee, J.-H. Lee, M. Kim and Y.-C. Joo, *RSC Adv.*, 2021, 11, 8198
40. J. Liu, J. Wang, B. Zhang, Y. Ruan, H. Wan, X. Ji, K. Xu, D. Zha, L. Miao and J. Jiang, *J. Mater. Chem. A*, 2018, 6, 2067